Article

A new amide proton $R_{1\rho}$ experiment permits accurate characterization of microsecond time-scale conformational exchange

Christian Eichmüller & Nikolai R. Skrynnikov*
Department of Chemistry, Purdue University, 560 Oval Drive, West Lafayette, IN, 47907-2084, USA

Abstract

A new off-resonance spin-lock experiment to record relaxation dispersion profiles of amide protons is presented. The sensitivity-enhanced HSQC-type sequence is designed to minimize the interference from cross-relaxation effects and ensure that the dispersion profiles in the absence of μs-ms time-scale dynamics are flat. Toward this end (*i*) the proton background is eliminated by sample deuteration (Ishima et al., 1998), (*ii*) ^{1}H spin lock is applied to two-spin modes $2(H_x \sin\theta + H_z \cos\theta)N_z$, and (*iii*) the tilt angle $\theta \approx 35°$ is maintained throughout the series of measurements (Desvaux et al., 1995). The relaxation dispersion profiles recorded in this manner sample a wide range of effective rf field strengths (up to and in excess of 20 kHz) which makes them particularly suitable for studies of motions on the time scale ≤ 100 μs. The new experiment has been tested on the Ca^{2+}-loaded regulatory domain of cardiac troponin C. Many residues show pronounced dispersions with remarkably similar correlation times of ~30 μs. Furthermore, these residues are localized in the regions that have been previously implicated in conformational changes (Spyracopoulos et al., 1997).

Introduction

Nuclear magnetic resonance (NMR) spectroscopy has become a powerful tool for probing dynamics of biological macromolecules on a wide range of time scales. Over the last 15 years a number of strategies have been developed to measure various auto- and cross-relaxation rates and interpret the data in terms of molecular motions (Palmer, 2004). The results of these studies have contributed substantially to our understanding of biomolecular systems.

Of all the motional time scales amenable to NMR studies, the micro- to millisecond range is especially important from a biological perspective.

Recent relaxation dispersion studies in this field provided insight into molecular mechanisms of enzymatic catalysis (Ishima et al., 1999; Wang et al., 2001b; Eisenmesser et al., 2002), regulation of ligand binding (van Tilborg et al., 2000; Kristensen et al., 2000; Tolkatchev et al., 2003) including entropy-driven cooperativity effects (Stevens et al., 2001; Yung et al., 2003), the origin of protein stability (Mulder et al., 2001; Butterwick et al., 2004), and folding pathways (Grey et al., 2003; Korzhnev et al., 2004; Kuwata et al., 2004; Platt et al., 2005).

Motions in the micro- to millisecond timeframe lead to modulation of isotropic chemical shifts and thus give rise to broadening of spectral lines. The Redfield-theory treatment of this effect, when applicable, determines the corresponding contribution to transverse relaxation rate, R_{ex}. Since

*To whom correspondence should be addressed. E-mail: nikolai @purdue.edu

chemical shift evolution can be partially or fully refocused by application of rf fields, the magnitude of R_{ex} decreases under spin-lock conditions. Measurements of R_{ex} in the presence of an rf field of variable strength provides, therefore, an efficient tool for studies of μs-ms motions.

Most of the work in this field has focused on ^{15}N spin probe, with only a few studies making use of ^{1}H probe (Ishima et al., 1998, 1999; Kojima et al., 2001; Ishima and Torchia, 2003). The lack of proton data is especially conspicuous given the potential benefits from such measurements. Indeed, proton chemical shifts in proteins are better indicators of the tertiary structure than heteronuclear shifts (Ösapay and Case, 1991; Asakura et al., 1995). This makes them potentially highly useful for modeling the structure of transient ('excited') states (Mulder et al., 2001). Note that relaxation dispersion measurements are often the only source of information on sparsely populated 'excited' states since these states cannot be directly observed in the spectra or adequately characterized by NOE data. An additional argument for the use of proton dispersions is the high gyromagnetic ratio of protons which makes it possible to generate much stronger effective rf fields. This facilitates the studies of faster exchange processes (Ishima and Torchia, 2003).

The reason for the limited use of ^{1}H dispersion experiments lies, primarily, in the complicated relaxation behavior of protons. Protons inside a protein form an extensive relaxation-coupled network (Kalk and Berendsen, 1976). In this situation the outcome of the spin-lock relaxation experiment shows a complex dependence on the strength of the applied rf field. We use the term *pseudo-dispersion* to describe the variation of $R_{1\rho}$ with the strength of rf field ω_1 which has its origin in dipolar cross-relaxation and not in R_{ex}. For example, consider a series of off-resonance experiments where the direction of the effective rf field changes from x to nearly z. The proton relaxation context changes accordingly from ROE to NOE which brings about pronounced pseudo-dispersion effects. In order to counter these effects we implemented the following three strategies:

(*i*) *Use of deuterated sample*. Deuteration of non-labile proton sites has a long history in protein NMR (Matthews et al., 1977; LeMaster, 1987; Torchia et al., 1988). In their ground-breaking relaxation dispersion experiment, Ishima and Torchia used a deuterated sample with protons introduced in amide positions via exchange with solvent (Ishima et al., 1998). The high degree of deuteration eliminates Hartmann-Hahn (TOCSY) transfer between scalarly coupled protons that otherwise causes severe pseudo-dispersion effects. Furthermore, deuteration leads to a substantial drop in the $^{1}H^{N}$ relaxation rates which facilitates the observation of R_{ex} terms. Finally, deuteration greatly dilutes the proton pool and therefore reduces the pseudo-dispersion effects associated with cross-relaxation. Nonetheless, the remaining cross-relaxation among $^{1}H^{N}$ and other protons (appearing due to exchange with solvent and incomplete deuteration) is sufficient to compromise the relaxation dispersion measurements. This problem can be circumvented when both sample and solvent have a very high proportion of deuterium (e.g. 98–99%), but at the expense of dramatic decrease in sensitivity (Ulmer et al., 2004).

(*ii*) *Use of selective initial conditions*. In the situation when only one magnetization mode out of many is excited, the relaxation initially proceeds in a selective fashion, i.e. it is insensitive to cross-relaxation effects over short t_{rel} intervals. On the other hand, at longer t_{rel} intervals the combination of selective initial conditions with ROE cross-relaxation transfer ensures a relatively slow magnetization decay which is advantageous for R_{ex} measurements. The experiment by Ishima and Torchia relies on 'dephasing' of individual proton magnetizations during the evolution time to generate selective initial conditions (Ishima et al., 1998). In this work we demonstrate how two-spin proton-nitrogen modes can be used to enforce the selective relaxation regime. The selective conditions are superior to non-selective in that they help to minimize the pseudo-dispersion effects.

(*iii*) *Constant tilt angle measurements*. For a large molecule in the slow tumbling limit cancellation of NOE and ROE cross-terms occurs when the spin magnetizations are locked at the angle $\theta = \arctan(1/\sqrt{2}) = 35.3°$. This property has been previously exploited in a number of different applications (Griesinger and Ernst, 1987; Cavanagh and Rance, 1992; Hwang et al., 1997). Clearly, it can also be used to minimize the pseudo-dispersion effects associated with cross-relaxation. Desvaux and co-authors proposed an experiment where the strength of the rf field, ω_1, and the rf carrier offset, Ω, are changed in concert

such that the angle θ is maintained constant, $\theta = 35.3°$ (Desvaux et al., 1995). Note that the angle $\theta = 35°$ represents a good choice for off-resonance measurements. Indeed, on one hand it produces large effective rf fields, $\omega_1^{\text{eff}} = \sqrt{3}\omega_1$, while on the other hand it retains sufficiently large transverse magnetization component which ensures good sensitivity toward R_{ex}. In addition, the small amount of TOCSY transfer that may be present due to residual $^1H^\alpha$ content is essentially eliminated at $\theta = 35°$ (Brüschweiler et al., 1989). Here we implement the concept of a constant tilt angle experiment for the two-spin proton-nitrogen modes. In order to minimize the effect of the spread in $^1H^N$ chemical shifts and ensure $\theta \approx 35°$ conditions for all amide protons we combine the results of the two measurements where the rf field carrier is placed up- and down-field from the center of $^1H^N$ spectrum (Schleucher et al., 1995; Desvaux and Goldman, 1996). An additional improvement is obtained from the use of the constant relaxation time scheme (Akke and Palmer, 1996).

In this work we utilize concepts (*i–iii*) to design a clean, simple, and sensitive experiment for measuring $^1H^N$ relaxation dispersions. The application to Ca^{2+}-loaded N-terminal domain of cardiac troponin C (Ca^{2+}-NcTnC) is presented. A dynamic process with characteristic time $\sim$30 μs (12.4 °C) has been identified in this system using the results from proton dispersion measurements. The results are in good agreement with the motional model developed by Sykes and others (Spyracopoulos et al., 1997; Pääkkönen et al., 1998; McKay et al., 2000).

Pulse sequence for recording proton dispersions

The new pulse sequence shown in Figure 1 allows recording of off-resonance $R_{1\rho}$ proton relaxation dispersion profiles. The sequence is a standard sensitivity-enhanced ^{15}N-HSQC (Kay et al., 1992; Schleucher et al., 1993) with an inserted relaxation period which extends from point a to point b in the scheme. Following point a, the magnetization $H_z N_z$ is aligned with the effective proton spin-lock field by means of an adiabatic half-passage pulse (Garwood and Ke, 1991; Mulder et al., 1998). The resulting coherence, $(H_x \sin\theta + H_z \cos\theta)N_z$, relaxes under proton spin-lock conditions for a period of time t_{rel} before being restored to $H_z N_z$ by means of a time-reversed half-passage pulse. This is followed by a relaxation compensation period of duration $T - t_{\text{rel}}$ that extends to point b in the sequence (Akke and Palmer, 1996).

In what follows we concentrate on the relaxation behavior of the spin system during the spin-lock period t_{rel}. We begin by considering proton cross-relaxation and its effect on the dispersion profiles, and later discuss the exchange term, R_{ex}.

The coherence of interest during the spin-lock period of the pulse sequence Figure 1 can be represented as $V^{(n,n)} = (H_x^n \sin\theta + H_z^n \cos\theta)N_z^n$, where index n denotes the residue number. It is straightforward to show that there is no cross-relaxation between the coherences from two residues, $V^{(n,n)}$ and $V^{(i,i)}$. However, there are cross-relaxation terms that couple $V^{(n,n)}$ to $V^{(i,n)}$, where the latter represents the correlation between the ^{15}N spin from residue n and the $^1H^N$ spin from residue i, $V^{(i,n)} = (H_x^i \sin\theta + H_z^i \cos\theta)N_z^n$. This coherence is somewhat unusual in that it is long-range and accessible only via cross-relaxation transfer, and not via scalar coupling.

Thus, the operator basis required for the analysis of the amide group n is comprised of the coherences $V^{(i,n)}$ where i runs over all non-proline residues in the protein, $i = 1,2,\ldots ,n,\ldots$ (for the moment we assume that only amide sites contain protons). The relaxation matrix elements $\Gamma_{ij}^{(n)}$ evaluated in this basis are listed below:

$$\Gamma_{ii}^{(n)} = (R_{\text{anti}} + R_{\text{ex}})\sin^2\theta_i + R_{zz}\cos^2\theta_i$$

$$R_{\text{anti}} = R_{2,Hx}^{H,\text{CSA}} + R_{1,Nz}^{N,\text{CSA}} + \delta_{ni}R_{HxNz}^{HN,\text{dip}}$$
$$+ \sum R_{2,Hx}^{HH,\text{dip}}$$

$$R_{zz} = R_{1,Hz}^{H,\text{CSA}} + R_{1,Nz}^{N,\text{CSA}} + \delta_{ni}R_{HzNz}^{HN,\text{dip}}$$
$$+ \sum R_{1,Hz}^{HH,\text{dip}} \qquad (1)$$

$$\Gamma_{ij}^{(n)} = R_{NOE}^{HH,\text{dip}}\cos\theta_i \cos\theta_j$$
$$+ R_{ROE}^{HH,\text{dip}}\sin\theta_i \sin\theta_j \quad (i \neq j) \qquad (2)$$

The relaxation terms comprising R_{anti} and R_{zz} are defined in a standard fashion (Peng and Wagner, 1992) and include the summation over all proximal protons. Note that dipolar auto-relaxation contributions $R^{HN,\text{dip}}$ are zero in all elements of $\Gamma^{(n)}$

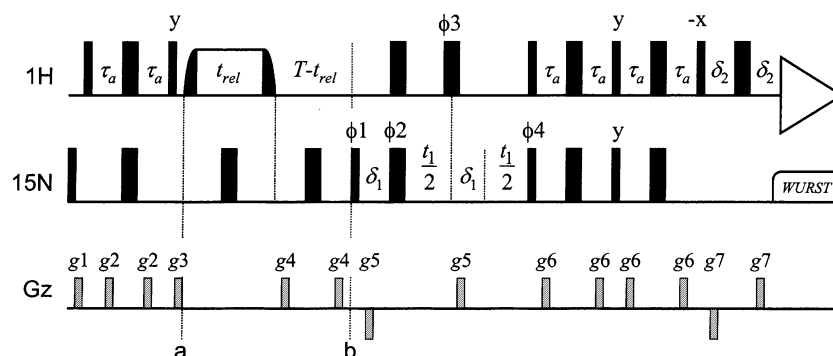*Figure 1.* Pulse sequence for $^1H^N$ relaxation dispersion measurements. All narrow (wide) rectangular pulses are applied with a flip angle of 90° (180°) along the *x*-axis unless indicated otherwise. The spin-lock period t_{rel} is flanked by adiabatic half-passage pulses (amplitude tailored according to the *tanh* function, frequency sweep controlled by the *tan* function, sweep width 100 kHz, duration 4 ms, the two half-passage pulses are related via time reversal (Mulder et al., 1998)). These pulses are integrated in the spin-lock period such that their maximum amplitude is equal to the spin-lock amplitude (up to 12.3 kHz). The proton rf field is applied at water line, except for the interval between points *a* and *b* where the carrier is positioned at 8.19 ppm $\pm \Delta$. Nitrogen decoupling during the acquisition is achieved using a WURST sequence (Kupce and Freeman, 1995) with maximum rf field strength of 1.2 kHz. The phase cycle is: $\phi_1 = \{x, -x\}$, $\phi_2 = \{2x, 2y, 2(-x), 2(-y)\}$, $\phi_3 = \{x\}$, $\phi_4 = \{x\}$, and $rec = \{x, -x, -x, x\}$. Quadrature detection in F1 is achieved using the sensitivity enhancement scheme (Kay et al., 1992; Schleucher et al., 1993) by recording two datasets with (ϕ_4, g5) and ($\phi_4 + 180°$, −g5) for each t_1 increment. Phase ϕ_1 is incremented in concert with receiver phase to shift axial peaks to the edge of the spectrum (Marion et al., 1989) Gradient pulses g1 to g7 are applied with durations 1.0, 0.5, 1.0, 1.0, 1.25, 0.5, and 0.125 ms and amplitudes 5.0, 4.0, 20.0, 12.0, 15.0, 4.0, and 14.86 G/cm, respectively. The delays are $\tau_a = 2.25$ ms, $\delta_1 = 1.5$ ms, $\delta_2 = 0.5$ ms.

except $\Gamma_{nn}^{(n)}$ because of the long distances between ^{15}N and $^1H^N$ residing in different residues (as indicated by the Kronecker delta, δ_{ni}, in Eq. (1)). For the same reason we can safely neglect cross-correlated dipole-dipolar contributions into $\Gamma_{ij}^{(n)}$ (not listed in Eq. (2)). $^1H^N$-^{15}N dipolar – $^1H^N$ CSA cross-correlations are suppressed in a standard fashion by applying a nitrogen 180° pulse during t_{rel} (Palmer et al., 1992; Korzhnev et al., 2002). We choose, however, not to suppress $^1H^N$-^{15}N dipolar – ^{15}N CSA cross-correlations to avoid interfering with the spin lock. These cross-correlated terms are of longitudinal type, i.e. relatively small; our simulations indicate that they have vanishingly small effect (less than 0.1 s^{-1}) on the obtainable dispersion profiles.

Equations (1) and (2) set the stage for a complete relaxation matrix analysis similar to the treatment of off-resonance ROESY (Kuwata et al., 1997). Unlike in the standard procedure, however, the coherences of interest represent two-spin operators. Importantly, in the context of two-spin modes the relaxation occurs in a *selective* manner. Indeed, while the coherence $V^{(n,n)}$ is excited at the beginning of the spin-lock period, other coherences $V^{(i,n)}(i \neq n)$ at this point are strictly zero (which is the equilibrium value for

two-spin modes). Note also that complete relaxation matrix analysis should be executed for each amide group individually since the matrices $\Gamma^{(n)}$ differ with regard to the placement of $R^{HN,dip}$ term as discussed above.

As described in the introduction, the sequence Figure 1 is intended to be run with the fixed θ value, $\theta = 35°$. If this condition is met and if the system is in the slow tumbling regime, then cross-relaxation terms, Eq. (2), disappear. The relaxation of $V^{(n,n)}$ in this case is monoexponential and can be directly used to monitor proton dispersions. Specifically, a series of measurements can be performed using the sequence Figure 1 where the rf carrier offset and the strength of rf field are changed in concert such that $\Omega = \sqrt{2}\omega_1$. The relaxation rate obtained in this experiment, Eq. (1), consists of two parts: R_{ex} which is sensitive to the magnitude of the effective rf field,

$$\omega_1^{eff} = \sqrt{\omega_1^2 + \Omega^2} = \sqrt{3}\omega_1,$$ and all other terms that remain constant provided that θ does not change. Thus, the relaxation dispersion profile can be recorded in this fashion (Desvaux et al., 1995).

One technical difficulty remains to be addressed, however. Given the spread in $^1H^N$ chemical shifts, it is strictly speaking not possible to lock all spin

modes at $\theta = 35°$, especially when ω_1 is relatively weak. In order to deal with this problem, we implemented two solutions: a constant relaxation time scheme and the symmetric placement of the rf carrier relative to the center of the $^1H^N$ spectrum.

The constant relaxation time scheme (Akke and Palmer, 1996; Wang et al., 2001a), where peak intensities are monitored as a function of t_{rel}, yields the following observable decay rates:

$$R_{1\rho}^{obs} = (R_{anti} + R_{ex})\sin^2\theta + R_{zz}\cos^2\theta - R_{zz}^{eff}$$

$$(3)$$

In formulating this result we assume that θ is reasonably close to $35°$ so that the cross-relaxation effects, Eq. (2), can be neglected during the time t_{rel}. On the other hand, during the interval $T - t_{rel}$ cross-relaxation is active so that the effective decay rate R_{zz}^{eff} is, generally speaking, different from R_{zz}, Eq. (1).

Since θ can deviate somewhat from the desired value of $35°$, the effect of these deviations is minimized by computing a modified rate (Akke and Palmer, 1996):

$$R_{1\rho}^{mod} = R_{1\rho}^{obs}/\sin^2\theta = (R_{anti} - R_{zz} + R_{ex})$$
$$+ (R_{zz} - R_{zz}^{eff})/\sin^2\theta \quad (4)$$

In $R_{1\rho}^{mod}$ the dependence on θ appears in the last term, which is small. Indeed, R_{zz}^{eff} describes the *selective* relaxation of $H_z N_z$ over a relatively short period of time $T - t_{rel}$ (T is chosen to accommodate a faster relaxation process, R_{anti}). As a result, cross-relaxation effects have little impact on R_{zz}^{eff} and the difference $R_{zz} - R_{zz}^{eff}$ is small (confirmed by numerical simulations; see below). This ensures

that $R_{1\rho}^{mod}$ is to a good approximation insensitive to small variations in θ.

On top of the constant relaxation time scheme we implement yet another solution (Schleucher et al., 1995; Desvaux and Goldman, 1996) to bring the system closer to the desired $\theta = 35°$ conditions. Specifically, two copies of the spectrum are recorded: with rf field carrier set up- and down-field from the center of $^1H^N$ region. The scheme is illustrated in Figure 2, where ω_{ref} is the center of $^1H^N$ region (8.19 ppm in our experimental study) and ω is the carrier frequency, $\omega = \omega_{ref} \pm \Delta$. The magnitude of the offset Δ is varied according to $\Delta = \sqrt{2}\omega_1$ so that the $\theta = 35°$ condition is strictly met for a proton resonating at ω_{ref}. On the other hand, for a peak that resonates at ω_0 (shown in Figure 2) two experiments with symmetric positioning of the carrier result in two distinct tilt angles, $\theta_+ < 35° < \theta_-$, and ultimately in two distinct rates, $R_{1\rho,\pm}^{mod}$. Inasmuch as the problem can be linearized over a small interval in θ and ω_1^{eff} (Desvaux and Goldman, 1996), the averaging of the two rates effectively achieves the $\theta = 35°$ condition. Hence, we suggest the following data processing scheme:

$$\bar{R}_{1\rho}^{mod} = (R_{1\rho,+}^{mod} + R_{1\rho,-}^{mod})/2 = \left(\frac{R_{1\rho,+}^{obs}}{\sin^2\theta_+} + \frac{R_{1\rho,-}^{obs}}{\sin^2\theta_-}\right)\Big/2$$

$$(5)$$

$$\bar{\omega}_1^{eff} = (\omega_{1,+}^{eff} + \omega_{1,-}^{eff})/2$$
$$= \left(\sqrt{\Omega_+^2 + \omega_1^2} + \sqrt{\Omega_-^2 + \omega_1^2}\right)\Big/2 \quad (6)$$

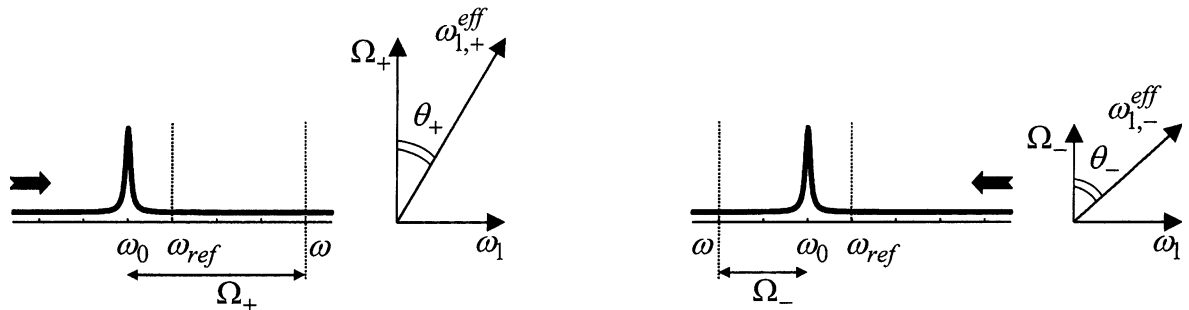*Figure 2.* Symmetric placement of the rf carrier, $\omega = \omega_{ref} \pm \Delta$, in the off-resonance spin-lock experiment Figure 1. Consider an example where $(\omega_0 - \omega_{ref})/2\pi = 0.5$ kHz, $\omega_1/2\pi = 3.0$ kHz, $\Delta = |\omega - \omega_{ref}| = \sqrt{2}\omega_1$. The two complementary tilt angles in this case are $\theta_+ = 32.3°$ and $\theta_- = 38.7°$. This corresponds to the effective mean angle of $35.5°$ which is very close to the desired value of $35.3°$. (While it makes no difference for the present experimental scheme, in general Ω should be treated as a signed quantity and the θ angles should be determined using the four-quadrant *arctan* function).

where $\theta_\pm$ and $\Omega_\pm$ are determined for individual peaks based on the $^1H^N$ chemical shift values. It should be noted that the experiment is run in an interleaved manner so that $R_{1\rho,+}^{obs}$ and $R_{1\rho,-}^{obs}$ are obtained concurrently. For both tilt angles, θ_+ and θ_-, adiabatic pulses achieve near-perfect alignment of the magnetization with the effective rf field.

The results Equations (1–6) establish a framework for analyzing the outcome of the experiment Figure 1. In order to verify that the proposed scheme eliminates pseudo-dispersion effects we undertook a series of numerical simulations. At first, the data were simulated in the absence of chemical exchange, $R_{ex} = 0$, so that the dispersion profiles $\bar{R}_{1\rho}^{mod}(\bar{\omega}_1^{eff})$ were expected to be flat. The high-resolution NMR structure of Ca^{2+}-loaded N-terminal domain of cardiac troponin C PDB-Id 1AP4 (Spyracopoulos et al., 1997) was used for the simulations. A version of the complete relaxation matrix analysis based on Equations (1, 2) supplemented with selective initial conditions was performed for each residue in the protein. In addition to the backbone $^1H^N$, the exchangeable side-chain protons were included in the analyses. The relaxation rates $R_{1\rho}^{obs}$ were evaluated from the simulated peak intensities at two points, $t_{rel} = 0$ and $t_{rel} = T$, where T was adjusted for each individual residue to obtain a reasonable amount of decay. The rates $\bar{R}_{1\rho}^{mod}$ were subsequently calculated according to Eqs. (5, 6). $^1H^N$ chemical shifts used in these calculations were taken from the experimental data (Spyracopoulos et al., 1997). In the case of exchangeable side-chain protons, chemical shift values were obtained from SHIFTX (Neal et al., 2003).

Figure 3 shows the three *worst* (i.e. farthest from flat) dispersion profiles simulated for Ca^{2+}-NcTnC. In each of these cases, pseudo-dispersion is caused by a combination of strong cross-relaxation and 'extreme' chemical shifts. In Asp-62, $^1H^N$ interacts with a nearby proton from a glutamine side chain (interproton distance 2.04 Å) whose chemical shift is at the low end of the amide range (6.8 ppm). In a pair of sequential residues, Ser-69 and Gly-70, there is a strong interaction between the two amide protons (2.35 Å) and the $^1H^N$ resonance of Gly-70 is shifted far downfield (10.8 ppm). These are the most unfavorable cases, which provide a stringent test for our experimental scheme. Nonetheless, the simulated relaxation dispersion profiles are entirely satisfactory: the magnitude of the pseudo-dispersion effects does not exceed 2.5 s^{-1}, and starting from
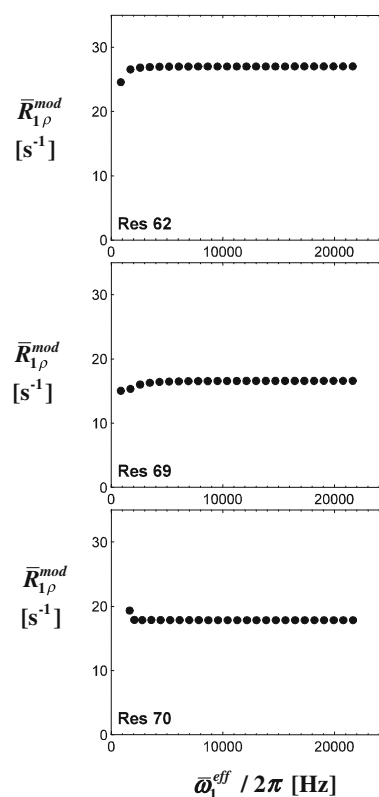

Figure 3. Relaxation dispersion profiles simulated for the experiment Figure 1. The curves in the absence of chemical exchange are expected to be flat. The simulations used the coordinates PDB-Id 1AP4 of Ca^{2+}-NcTnC (first structure from the ensemble) (Spyracopoulos et al., 1997). Of all the dispersion curves simulated for 86 non-proline residues, the three *worst* (i.e. farthest from flat) profiles are shown in the plot. The calculations assumed operational frequency $\omega_0/2\pi = 600$ MHz, rotational correlation time $\tau_{rot} = 10$ ns, rf field range $\omega_1/2\pi = 0.5 - 12.5$ kHz, and solvent composition 90% H_2O – 10% D_2O. The complete relaxation matrix analysis was carried out for each individual amide group in Ca^{2+}-NcTnC and the relaxation rates $\bar{R}_{1\rho}^{mod}$ were evaluated from the intensities of simulated peaks at $t_{rel} = 0$ and $t_{rel} = T$. The delays T were adjusted to 66, 115, and 103 ms for Asp-62, Ser-69, and Gly-70, respectively, to ensure the decay of magnetization to the level of 30%. A total of 136 protons were included in the simulations. Backbone $^1H^N$ spins and $^1H^{\delta21/\delta22}$, $^1H^{\epsilon21/\epsilon22}$ spins from asparagine and glutamine side chains were represented by the modes $V^{(i,n)}$. With regard to other labile protons such as Ser/Thr $^1H^\gamma$, Lys $^1H^\zeta$, etc., we note that under the present experimental conditions (pH 7) they undergo fast exchange with solvent (Wüthrich, 1986) so that the corresponding modes $V^{(i,n)}$ rapidly decay (Skrynnikov and Ernst, 1999) and therefore effectively 'self-decouple'. Consequently, these protons were taken into account only in calculating $R^{HH,dip}$ auto-relaxation rates. Finally, note that although the described simulations provide a realistic picture of the pseudo-dispersion effects they are unlikely to achieve a quantitative agreement with the experimental data because of the uncertainty in interproton distances.

$\bar{\omega}_1^{\text{eff}}/2\pi \sim 2.5$ kHz the profiles are practically flat. It is noteworthy that no other residues in our simulations show pseudo-dispersion effects in excess of 1 s^{-1}, and for the large majority the effect is less than 0.1 s^{-1}.

In the analyses described above we have established that the pulse sequence Figure 1 is, to a very good approximation, insensitive to cross-relaxation effects. When $\theta = 35°$ the relaxation matrix $\Gamma^{(n)}$ is diagonal and the exchange contributions R_{ex} can be obtained directly from the measured relaxation rates, cf. Eq. (4). To demonstrate the robust nature of our approach with respect to dispersion measurements we repeated the simulations of Figure 3 with the exchange terms included. A simple two-site fast-exchange model was adopted:

$$R_{\text{ex}} = p_a p_b (\delta_a - \delta_b)^2 \omega_0^2 \frac{\tau_{\text{ex}}}{1 + (\omega_1^{\text{eff}}\tau_{\text{ex}})^2} \qquad (7)$$

where p_a and p_b are the populations of the two species, δ_a and δ_b are the intrinsic chemical shifts, and τ_{ex} is the exchange correlation time. The results (not shown) demonstrated that the target values of $p_a p_b (\delta_a - \delta_b)^2 \omega_0^2 = 1.3 \cdot 10^6$ s^{-2} and $\tau_{\text{ex}} = 30$ μs can be recovered from the simulated dispersion data with a very good accuracy. A small error, never exceeding 7%, is due to the residual pseudo-dispersion effects visible in Figure 3.

Finally, it is instructive to compare the usefulness of different elements used in our experimental strategy: sample deuteration, use of the two-spin modes, constant θ scheme, constant relaxation time scheme, and symmetric carrier placement. To address this problem, we carried out a series of simulations where these elements were removed, one at a time. The results are illustrated in the Supplementary Material in Figure S1. In brief, all the elements proved to be important; the absence of any one of them led to substantial increase in pseudo-dispersion effects. Especially important is the use of constant θ scheme. Of interest, less-than-complete deuteration has only modest deleterious effect on the dispersion profiles. In our simulations, at 75% deuteration level the amplitude of pseudo-dispersion did not exceed 4 s^{-1}, with the affected region extending to ca. 5 kHz. It is therefore conceivable that our experiment can be used with a wide range of samples (Fiaux et al., 2004), including lower-cost samples expressed in ^{15}N-enriched, D$_2$O-based minimal media.

Application to Ca^{2+}-loaded N-terminal domain of cardiac troponin C

Cardiac troponin C is a signaling protein that regulates heart muscle contraction. The 89-residue N-terminal domain of this protein has been extensively investigated by NMR methods. It has been suggested that upon binding the calcium ion NcTnC establishes a dynamic equilibrium involving closed and open forms. The open form apparently represents a transient state with low population that cannot be easily characterized. It has been directly observed, however, in the complex of Ca^{2+}-NcTnC with a fragment of troponin I (Li et al., 1999) and in the Ca^{2+}-loaded skeletal isoform of troponin C (Gagné et al., 1995). According to these data, the opening involves translocation of the two helices that move as a rigid unit. The hinge residues identified from structural analyses display significant nitrogen line-broadening in Ca^{2+}-NcTnC spectra (Spyracopoulos et al., 1998; Pääkkönen et al., 1998; Abbott et al., 2000). However, to the best of our knowledge, no relaxation dispersion studies have been performed on Ca^{2+}-NcTnC, and the time scale of the presumed conformational exchange remains unknown.

The pulse sequence Figure 1 was used to record proton relaxation dispersions in a 1.5 mM sample of Ca^{2+}-NcTnC at 12.4 °C. Figure 4 shows the regions of the spectral map recorded with $\omega_1/2\pi = 12.35$ kHz, $t_{\text{rel}} = 0$ (reference experiment) and $t_{\text{rel}} = T = 80$ ms. Despite the fact that the peaks showing the evidence of conformational exchange have low intensity (e.g. Ser-37 and Thr-38 in Figure 4), high-quality data have been obtained in a short period of time (1 h 15 min per HSQC plane which corresponds to a single point in the dispersion curve). The sample deuteration (Ishima et al., 1998), use of the ramped spin lock (Mulder et al., 1998), and the sensitivity enhancement scheme (Kay et al., 1992) all contribute to the high sensitivity of the experiment. The spectral maps contain only HSQC correlations and are free of any additional cross-peaks.

Using the experiment of Figure 1, proton relaxation dispersion data were obtained for 81 out of 89 residues (absent are two prolines, the N-terminal residue, and several severely overlapped signals). The data recorded at 600 and 800 MHz were fitted on a per-residue basis to one of the two models: straight line (two fitting
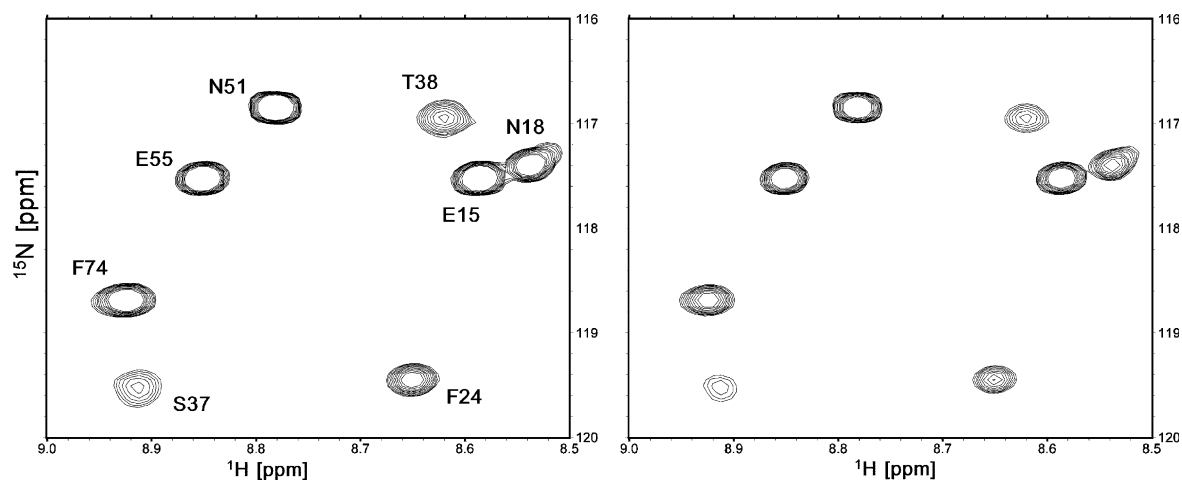
Figure 4. A region from the spectral map obtained with the pulse sequence of Figure 1. Experimental conditions: 1.5 mM sample of $^2H(^1H^N)$-, ^{15}N-labeled Ca^{2+}-NcTnC, temperature 12.4 °C, static field 600 MHz, room temperature probe, $\omega_1/2\pi = 12.35$ kHz. The spectra with $t_{rel} = 0$ (left panel) and $t_{rel} = T = 80$ ms (right panel) were recorded in 1 h 15 min each.

parameters, $R_{anti}^{600} - R_{zz}^{600}$ and $R_{anti}^{800} - R_{zz}^{800}$) or Lorentzian curve, Eq. (7) (four fitting parameters, $p_a p_b(\delta_a - \delta_b)^2$, τ_{ex}, $R_{anti}^{600} - R_{zz}^{600}$ and $R_{anti}^{800} - R_{zz}^{800}$). The Akaike information criterion was used to determine which of the two models is appropriate (Motulsky and Christopoulos, 2004). The data from *all 81 residues*, together with fitted curves and best-fit values of $p_a p_b(\delta_a - \delta_b)^2$ and τ_{ex}, are shown in the Supplementary material.

Of all the measured residues, 20 display statistically significant dispersions and the remaining 61 are perfectly flat. Figure 5 shows examples of the five residues with largest dispersions (i.e. highest fitted $p_a p_b(\delta_a - \delta_b)^2$ values). In addition, this figure shows a typical fit where there is no evidence of dispersion. In order to produce this typical example, the data from all residues were sorted according to the fit rmsd χ^2 and one residue, Ala-22, was picked precisely from the middle of the list. Of note, the five residues showing dispersions in Figure 5 report very similar τ_{ex} values, 27–30 μs. In fact, 16 out of 20 available dispersion curves yield τ_{ex} between 24 and 32 μs (four other curves produce somewhat higher τ_{ex} values, see Table S1). This is a remarkable degree of agreement which strongly points toward a concerted motion such as envisioned in the previous studies (Pääkkönen et al., 1998; McKay et al., 2000).

The largest dispersion effects, Figure 5, are observed at the sites that have been previously identified as dynamic: hinge residues associated with opening-closure (Leu-41, Val-64) and the so-called defunct Ca^{2+}-binding site (Leu-29, Gly-30) (Spyracopoulos et al., 1998; Pääkkönen et al., 1998). In Figure 6 we mapped the determined $p_a p_b(\delta_a - \delta_b)^2$ values onto three-dimensional structure of Ca^{2+}-NcTnC (PDB-Id 1AP4, closed conformation). Both hinge regions (marked by arrows) and the defunct calcium-binding site (dashed outline) appear as hot spots in the plot. The structural ramifications of these findings are currently under investigation and the results will be reported elsewhere.

While there is no straightforward way to separate p_a and $p_b = 1 - p_a$ from $\delta_a - \delta_b$ in the case of fast chemical exchange, some instructive estimates can be easily obtained. Given the conformity of the τ_{ex} values, it can be suggested that the motion occurs as a true two-site exchange characterized by a single p_a value. Assuming for the moment that $p_a = 0.2$, we obtain $\delta_a - \delta_b$ values in the range from 0.2 to 0.7 ppm for twenty residues showing statistically significant proton dispersions (see Table S1). These $\delta_a - \delta_b$ values appear to be reasonable given the scale of changes in chemical shifts observed upon calcium titration (Li et al., 1999). Previously, McKay et al. estimated that the open state of Ca^{2+}-NcTnC may be populated at the level of 5–15% (McKay et al., 2000).

For the sake of comparison, we also recorded a ^{15}N off-resonance $R_{1\rho}$ experiment. The standard pulse sequence (Korzhnev et al., 2002) with an
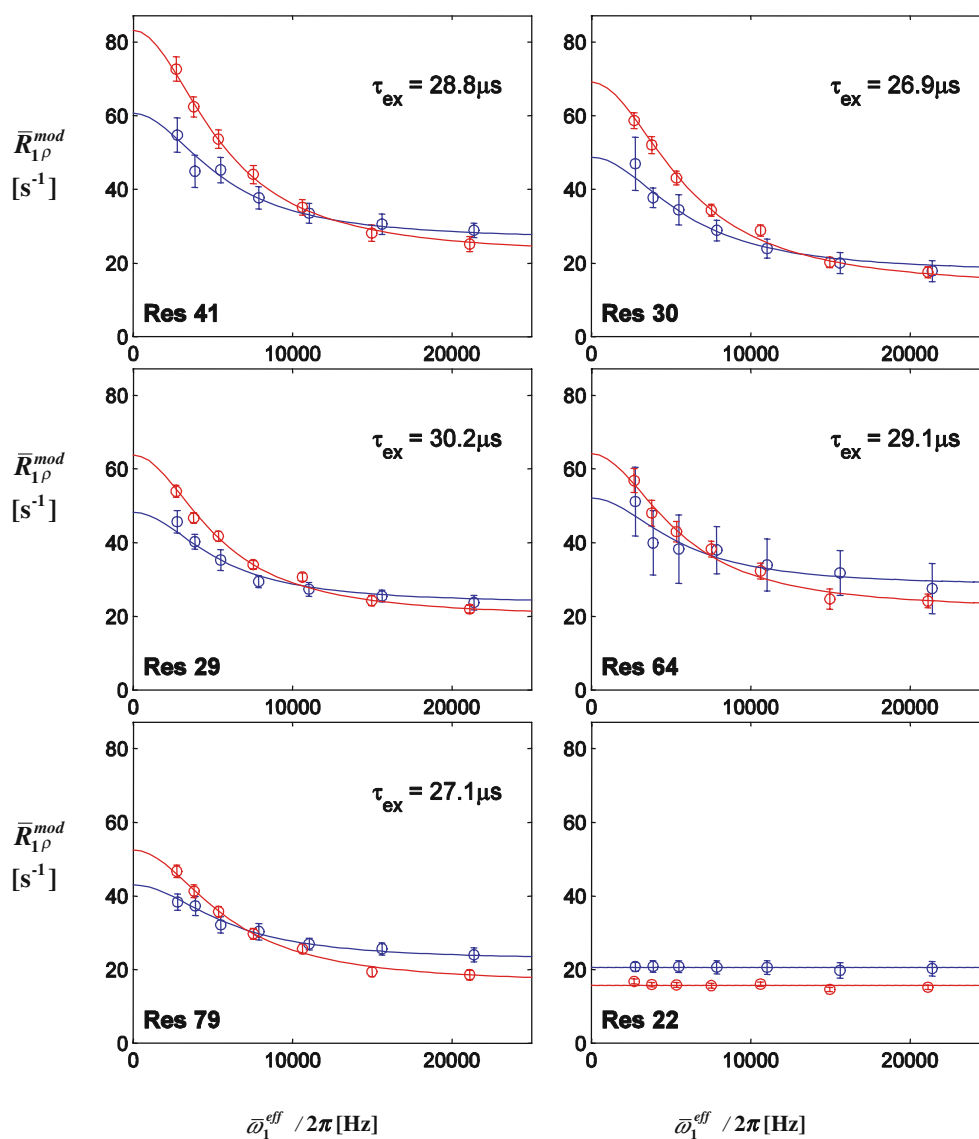
Figure 5. Proton relaxation dispersion profiles measured in ^{2}H(^{1}H^N)-, ^{15}N-labeled Ca^{2+}-NcTnC at 600 and 800 MHz (blue and red symbols, respectively). The data are for the five residues showing the largest dispersion effects, plus a single representative residue which has no detectable dispersion (Ala-22). Monte-Carlo simulations have been performed for each residue to determine the uncertainty in the fitted parameters (see Materials and methods for details). At the 90% confidence level, the following confidence intervals were obtained for τ_{ex}: 25–35 μs (Leu-41), 23–32 μs (Gly-30), 26–34 μs (Leu-29), 19–52 μs (Val-64), and 24–31 μs (Val-79). The data for all residues in Ca^{2+}-NcTnC can be found in the Supplementary Materials.

added ramped ^{15}N spin lock (Mulder et al., 1998) was used for these measurements. Clearly, due to the low gyromagnetic ratio, the magnitude of ω_1 for nitrogen is much lower than for protons. In our measurements the limiting rf field strength was 1.8 kHz for nitrogen vs. 12.3 kHz for protons (in fact, the proton power level could be comfortably raised further, whereas the nitrogen setting appeared close to a critical level).

The limited ω_1^{eff} range in ^{15}N experiments results in poor sampling of the dispersion curves which, in turn, leads to a large uncertainty in the τ_{ex} determination (Wang and Palmer, 2003). Note also that ^{15}N chemical shifts are relatively insen-
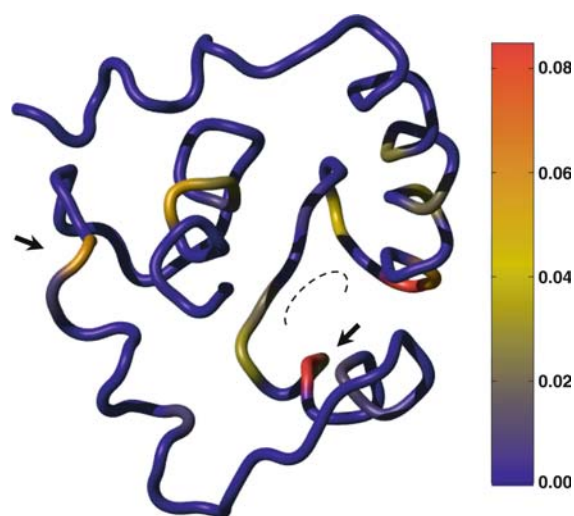
Figure 6. Main chain of Ca^{2+}-NcTnC (NMR structure 1AP4 (Spyracopoulos et al., 1997)) colored according to the values of $p_a p_b (\delta_a - \delta_b)^2$ obtained from the fitting of the proton relaxation dispersion data (Table S1). The hinge residues implicated in conformational exchange are indicated by the arrows and the defunct calcium-binding site is marked by a dashed contour. The figure was prepared using MOLMOL (Koradi et al., 1996).

sitive to changes in distant environment (Le and Oldfield, 1996). This restricts nitrogen dispersion observations to a handful of hinge residues where the changes in backbone dihedral angles are presumed to occur. The examples of such residues are Ser-37 and Thr-38 that give rise to weak peaks broadened both in the ^{15}N and ^{1}H dimensions (see Figure 4). Given the difficulties in studying ~ 30 μs dynamics with ^{15}N relaxation dispersion experiments, extra careful measurements are needed if quantitative analyses are intended. Such studies are currently underway in our group.

Concluding remarks

The proposed off-resonance spin-lock experiment allows for measurements of proton relaxation dispersion profiles over a wide range of ω_1^{eff}. If desired, the pulse sequence Figure 1 can also be executed as an on-resonance experiment with varied ω_1 and fixed rf carrier setting, $\Delta = 0$. Our simulations demonstrate that pseudo-dispersion effects remain small and the errors in the determination of $p_a p_b (\delta_a - \delta_b)^2$ and τ_{ex} are comparable to the $\theta = 35°$ experiment. On the other hand, an attempt to run the sequence with fixed ω_1 and

varied rf carrier offset Δ leads to severe pseudo-dispersion effects (observed both in simulations and experimentally). Thus, the use of the constant tilt angle is essential for the proposed experiment.

It is worth noting that the use of two-spin modes in the pulse sequence Figure 1 ensures selective relaxation conditions while at the same time avoiding the build-up of ROESY cross-peaks noted in other experimental schemes (Ishima et al., 1998). Indeed, the ROESY-type transfer in our experiment gives rise to long-range spin correlations that are never transformed into observables. It should also be pointed out that the auto-relaxation rates of the two-spin modes employed in this experiment are very similar to the rates of the corresponding single-spin proton modes. In our simulations we estimated that the difference between the two rates on average amounts to 1–2%, depending on the static field. Note also that two-spin modes decay to zero in off-resonance spin-lock measurements – unlike single-spin modes that relax toward a non-trivial equilibrium state (Desvaux and Goldman, 1994).

Comparing $^{1}H^{N}$ experiment with its ^{15}N counterpart, it can be argued that a proton constitutes a more versatile probe for conformational exchange. It is well-known that $^{1}H^{N}$ chemical shifts are more sensitive to the changes in distant environment (Ösapay and Case, 1991; Asakura et al., 1995). For instance, because of the higher gyromagnetic ratio of proton the shift of the $^{1}H^{N}$ resonances caused by the rearrangement of the side-chain aromatic rings is an order of magnitude larger than the corresponding ^{15}N shift. Analysis of ten randomly selected entries from BioMag-ResBank (Doreleijers et al., 2003) showed that the dispersion in chemical shifts of glycines, as expressed in the units of Hz, is 2.3 times greater in the $^{1}H^{N}$ dimension than in the ^{15}N dimension. After averaging over all types of amino acids, the ratio of 1.8 in favor of protons has been obtained. It is therefore expected that $^{1}H^{N}$ probe provides more extensive coverage of conformational changes compared to ^{15}N. Nitrogen chemical shifts, on the other hand, mainly depend on backbone torsional angles ψ and ϕ, and to a lesser extent on other factors (Le and Oldfield, 1996; Wishart and Nip, 1998). The two probes, therefore, can be viewed as complementary. It can be suggested, for example, that nitrogen measurements can be helpful in studying helix-coil transitions, whereas

proton dispersions are better suited for investigation of ligand binding or conformational exchange in the presence of paramagnetic centers. Furthermore, a combination of $^1H^N$ and ^{15}N probes (Kloiber and Konrat, 2000; Orekhov et al., 2004; Korzhnev et al., 2004) offers new insight into μs-ms time-scale events in proteins.

Materials and methods

Sample preparation

The C35S/C84S variant of N-terminal domain of human cardiac Troponin C, NcTnC, comprising residues 1–89 was expressed and purified as described previously (Li et al., 1995). NMR experiments were performed on a sample of 1.5 mM ^2H-, ^{15}N-labeled NcTnC in solution containing 6 mM $CaCl_2$, 10 mM imidazole (pH 7.0), 0.01% NaN_3, 90%H_2O, and 10%D_2O. The deuteration level of NcTnC obtained with Martek-9dN media (Spectra Stable Isotopes) was verified by mass spectrometry and estimated to be ∼97%.

NMR spectroscopy

The spectra were recorded at 12.4°C on Varian Unity Inova 600 and 800 MHz spectrometers equipped with room-temperature and cryogenic triple-resonance probes, respectively. The resonance assignments for C35S/C84S Ca^{2+}-NcTnC were kindly provided by Monica Li. The proton relaxation dispersion data were acquired using the pulse sequence shown in Figure 1. The 2D spectra at 600 MHz were recorded with spectral widths of 10,000 and 1800 Hz in the ^1H and ^{15}N dimensions, respectively, using a recycling delay of 2.0 s and 8 scans per t_1 increment. The data were stored as 960×128 complex matrices. Proton spin lock field strength was varied from 1.59 to 12.35 kHz (calibrated using a variable-width rectangular pulse inserted in the HSQC sequence). The rf carrier offsets relative to the center of the amide spectral region, 8.19 ppm, were adjusted according to $\Delta = \pm\sqrt{2}\omega_1$. Prior to the beginning of the spin-lock period the magnetization was aligned along the effective magnetic field using a 4 ms adiabatic half-passage pulse with a sweep width of 100 kHz (the directions of the sweep are shown with notched arrows in Figure 2) (Mulder et al., 1998).

The 800 MHz data were acquired with an essentially identical set of parameters. All experiments were recorded in an interleaved manner using (linked) arrays to increment ω_1, Δ, and t_{rel}. The script for separating the interleaved spectra is available upon request from the authors. To minimize the effects of rf heating, the ω_1 array was arranged in a random order and loaded in the innermost loop of the interleaved experiment (inside the t_1 cycle). In this manner, a thermal steady state is established and maintained in the sample throughout the experimental run. By examining $^1H^N$ chemical shifts in the series of spectra recorded on the Ca^{2+}-NcTnC sample, we found that the heating from the proton spin lock was, in fact, negligible (less than 0.1°C), which is consistent with the low ionic strength of the solvent.

The reference experiments ($t_{rel} = 0$) recorded with different ω_1 and Δ settings differ from each other only by the amplitude and carrier frequency of the adiabatic half-passage pulses. If the adiabatic pulses perform ideally then all reference spectra should be identical. Indeed, the deviations between multiple reference experiments were found to be less than 1%. Therefore, the measurements were conducted with reduced number of reference experiments (in principle, a single reference spectrum should suffice). The rates were obtained from peak intensities at two points, $t_{rel} = 0$ and $t_{rel} = T$. In a separate series of measurements with variable t_{rel} we verified that the decay curves are monoexponential.

As a sidenote, in the case of ∼ 1 ms time-scale exchange one has to be mindful of 'asymmetric' exchange contributions into $R_{1\rho,+}^{obs}$ and $R_{1\rho,-}^{obs}$ (Korzhnev et al., 2003).

Spectra processing

The spectra were processed using nmrPipe software (Delaglio et al., 1995). Lorentz-to-Gauss window function was applied in both dimensions and the data were zero-filled to 1024×512 complex points. The peaks were subsequently integrated using nlinLS (Delaglio et al., 1995). The following method was used for error analyses. The spectral map was divided into two halves, up- and downfield from the water signal. The upfield part of the spectrum, which contains nothing but spectral noise, was subjected to a cyclical shift in the ^{15}N dimension and then added to the left half. The

resulting spectrum was processed using nlinLS and the relaxation rates $\bar{R}_{1\rho}^{\mathrm{mod}}$ were obtained for all peaks. By repeating this procedure over a series of cyclical shifts we estimated the rmsd of $\bar{R}_{1\rho}^{\mathrm{mod}}$ due to spectral noise. The error bars in Figure 5 correspond to ± 1.96 of the rmsd values determined in this fashion. The advantage of this method is that it directly models the effect of spectral noise on the peak fitting procedure, thus leading to a more realistic representation of errors. The results were further used to estimate the uncertainty in the best-fit parameters such as τ_{ex}. Specifically, a series of Monte-Carlo simulations was conducted using the rmsd values described above. The confidence intervals containing 90% of the fitted τ_{ex} values were determined from these simulations.

Electronic Supplementary material is available at http://dx.doi.org/10.1007/s10858-005-0658-y

References

Abbott, M.B., Gaponenko, V., Abusamhadneh, E., Finley, N., Li, G., Dvoretsky, A., Rance, M., Solaro, R.J. and Rosevear, P.R. (2000) *J. Biol. Chem.*, **275**, 20610–20617.

Akke M. and Palmer A.G. (1996) *J. Am. Chem. Soc.* **118**, 911–912.

Asakura, T., Taoka, K., Demura, M. and Williamson, M.P. (1995) *J. Biomol. NMR*, **6**, 227–236.

Brüschweiler, R., Griesinger, C. and Ernst, R.R. (1989) *J. Am. Chem. Soc.*, **111**, 8034–8035.

Butterwick, J.A., Loria, J.P., Astrof, N.S., Kroenke, C.D., Cole, R., Rance, M. and Palmer, A.G. (2004) *J. Mol. Biol.*, **339**, 855–871.

Cavanagh, J. and Rance, M. (1992) *J. Magn. Reson.*, **96**, 670–678.

Delaglio, F., Grzesiek, S., Vuister, G.W., Zhu, G., Pfeifer, J. and Bax, A. (1995) *J. Biomol. NMR*, **6**, 277–293.

Desvaux, H., Birlirakis, N., Wary, C. and Berthault, P. (1995) *Mol. Phys.*, **86**, 1059–1073.

Desvaux, H. and Goldman, M. (1994) *Mol. Phys.*, **81**, 955–974.

Desvaux, H. and Goldman, M. (1996) *J. Magn. Reson. Ser. B*, **110**, 198–201.

Doreleijers, J.F., Mading, S., Maziuk, D., Sojourner, K., Yin, L., Zhu, J., Markley, J.L. and Ulrich, E.L. (2003) *J. Biomol. NMR*, **26**, 139–146.

Eisenmesser, E.Z., Bosco, D.A., Akke, M. and Kern, D. (2002) *Science*, **295**, 1520–1523.

Fiaux, J., Bertelsen, E.B., Horwich, A.L. and Wüthrich, K. (2004) *J. Biomol. NMR*, **29**, 289–297.

Gagné, S.M., Tsuda, S., Li, M.X., Smillie, L.B. and Sykes, B.D. (1995) *Nat. Struct. Biol.*, **2**, 784–789.

Garwood, M. and Ke, Y. (1991) *J. Magn. Reson.*, **94**, 511–525.

Grey, M.J., Wang, C. and Palmer, A.G. (2003) *J. Am. Chem. Soc.*, **125**, 14324–14335.

Griesinger, C. and Ernst, R.R. (1987) *J. Magn. Reson.*, **75**, 261–271.

Hwang, T.L., Mori, S., Shaka, A.J. and Zijl, P.C.M.van (1997) *J. Am. Chem. Soc.*, **119**, 6203–6204.

Ishima, R., Freedberg, D.I., Wang, Y.X., Louis, J.M. and Torchia, D.A. (1999) *Struct. Fold. Des.*, **7**, 1047–1055.

Ishima, R. and Torchia, D.A. (2003) *J. Biomol. NMR*, **25**, 243–248.

Ishima, R., Wingfield, P.T., Stahl, S.J., Kaufmann, J.D. and Torchia, D.A. (1998) *J. Am. Chem. Soc.*, **120**, 10534–10543.

Kalk, A. and Berendsen, H.J.C. (1976) *J. Magn. Reson.*, **24**, 343–366.

Kay, L.E., Keifer, P. and Saarinen, T.J. (1992) *J. Am. Chem. Soc.*, **114**, 10663–10665.

Kloiber, K. and Konrat, R. (2000) *J. Biomol. NMR*, **18**, 33–42.

Kojima, C., Ulyanov, N.B., Kainosho, M. and James, T.L. (2001) *Biochemistry*, **40**, 7239–7246.

Koradi, R., Billeter, M. and Wüthrich, K. (1996) *J. Mol. Graph.*, **14**, 51–55.

Korzhnev, D.M., Orekhov, V.Y., Dahlquist, F.W. and Kay, L.E. (2003) *J. Biomol. NMR*, **26**, 39–48.

Korzhnev, D.M., Salvatella, X., Vendruscolo, M., Di Nardo, A.A., Davidson, A.R., Dobson, C.M. and Kay, L.E. (2004) *Nature*, **430**, 586–590.

Korzhnev, D.M., Skrynnikov, N.R., Millet, O., Torchia, D.A. and Kay, L.E. (2002) *J. Am. Chem. Soc.*, **124**, 10743–10753.

Kristensen, S.M., Siegal, G., Sankar, A. and Driscoll, P.C. (2000) *J. Mol. Biol.*, **299**, 771–788.

Kupče, E. and Freeman, R. (1995) *J. Magn. Reson. Ser. A*, **115**, 273–276.

Kuwata, K., Kamatari, Y.O., Akasaka, K. and James, T.L. (2004) *Biochemistry*, **43**, 4439–4446.

Kuwata, K., Liu, H., Schleich, T. and James, T.L. (1997) *J. Magn. Reson.*, **128**, 70–81.

Le, H.B. and Oldfield, E. (1996) *J. Phys. Chem.*, **100**, 16423–16428.

LeMaster, D.M. (1987) *FEBS Lett.*, **223**, 191–196.

Li, M.X., Gagné, S.M., Tsuda, S., Kay, C.M., Smillie, L.B. and Sykes, B.D. (1995) *Biochemistry*, **34**, 8330–8340.

Li, M.X., Spyracopoulos, L. and Sykes, B.D. (1999) *Biochemistry*, **38**, 8289–8298.

Marion, D., Ikura, M., Tschudin, R. and Bax, A. (1989) *J. Magn. Reson.*, **85**, 393–399.

Matthews, K.S., Wade-Jardetzky, N.G., Graber, M., Conover, W.W. and Jardetzky, O. (1977) *Biochim. Biophys. Acta*, **490**, 534–538.

McKay, R.T., Saltibus, L.F., Li, M.X. and Sykes, B.D. (2000) *Biochemistry*, **39**, 12731–12738.

Motulsky, H. and Christopoulos, A. (2004) *Fitting Models to Biological Data Using Linear and Nonlinear Regression* Oxford University Press, New York.

Mulder, F.A., Mittermaier, A., Hon, B., Dahlquist, F.W. and Kay, L.E. (2001) *Nat. Struct. Biol.*, **8**, 932–935.

Mulder, F.A.A., Graaf, R.A.de, Kaptein, R. and Boelens, R. (1998) *J. Magn. Reson.*, **131**, 351–357.

Neal, S., Nip, A.M., Zhang, H.Y. and Wishart, D.S. (2003) *J. Biomol. NMR*, **26**, 215–240.

Orekhov, V.Y., Korzhnev, D.M. and Kay, L.E. (2004) *J. Am. Chem. Soc.*, **126**, 1886–1891.

Ösapay, K. and Case, D.A. (1991) *J. Am. Chem. Soc.*, **113**, 9436–9444.

Pääkkönen, K., Annila, A., Sorsa, T., Pollesello, P., Tilgmann, C., Kilpeläinen, I., Karisola, P., Ulmanen, I. and Drakenberg, T. (1998) *J. Biol. Chem.*, **273**, 15633–15638.

Palmer, A.G. (2004) *Chem. Rev.*, **104**, 3623–3640.

Palmer, A.G., Skelton, N.J., Chazin, W.J., Wright, P.E. and Rance, M. (1992) *Mol. Phys.*, **75**, 699–711.

Peng, J.W. and Wagner, G. (1992) *J. Magn. Reson.*, **98**, 308–332.

Platt, G.W., McParland, V.J., Kalverda, A.P., Homans, S.W. and Radford, S.E. (2005) *J. Mol. Biol.*, **346**, 279–294.

Schleucher, J., Quant, J., Glaser, S.J. and Griesinger, C. (1995) *J. Mag. Reson. Ser. A*, **112**, 144–151.

Schleucher, J., Sattler, M. and Griesinger, C. (1993) *Angew. Chem. Int. Ed. Engl.*,, **32**, 1489–1491.

Skrynnikov, N.R. and Ernst, R.R. (1999) *J. Mag. Reson.*, **137**, 276–280.

Spyracopoulos, L., Gagné, S.M., Li, M.X. and Sykes, B.D. (1998) *Biochemistry*, **37**, 18032–18044.

Spyracopoulos, L., Li, M.X., Sia, S.K., Gagné, S.M., Chandra, M., Solaro, R.J. and Sykes, B.D. (1997) *Biochemistry*, **36**, 12138–12146.

Stevens, S.Y., Sanker, S., Kent, C. and Zuiderweg, E.R.P. (2001) *Nat. Struct. Biol.*, **8**, 947–952.

Tilborg, P.J.A.van, Czisch, M., Mulder, F.A.A., Folkers, G.E., Bonvin, A.M.J.J., Nair, M., Boelens, R. and Kaptein, R. (2000) *Biochemistry*, **39**, 8747–8757.

Tolkatchev, D., Xu, P. and Ni, F. (2003) *J. Am. Chem. Soc.*, **125**, 12432–12442.

Torchia, D.A., Sparks, S.W. and Bax, A. (1988) *J. Am. Chem. Soc.*, **110**, 2320–2321.

Ulmer, T.S., Campbell, I.D. and Boyd, J. (2004) *J. Magn. Reson.*, **166**, 190–201.

Wang, C.Y., Grey, M.J. and Palmer, A.G. (2001a) *J.Biomol. NMR*, **21**, 361–366.

Wang, C.Y. and Palmer, A.G. (2003) *Magn. Reson. Chem.*, **41**, 866–876.

Wang, L.C., Pang, Y.X., Holder, T., Brender, J.R., Kurochkin, A.V. and Zuiderweg, E.R.P. (2001b) *Proc. Natl. Acad. Sci. USA*, **98**, 7684–7689.

Wishart, D.S. and Nip, A.M. (1998) *Biochem. Cell Biol.*, **76**, 153–163.

Wüthrich, K. (1986) *NMR of Proteins and Nucleic Acids* Wiley Interscience, New York.

Yung, A., Turnbull, W.B., Kalverda, A.P., Thompson, G.S., Homans, S.W., Kitov, P. and Bundle, D.R. (2003) *J. Am. Chem. Soc.*, **125**, 13058–13062.